energies

MDPI

Article

Experimental Study on the Acceleration Amplification Ratio of Cable Terminations for Electric Power Facilities

Bub-Gyu Jeon [1], Sung-Jin Chang [1], Sung-Wan Kim [1], Dong-Uk Park [1,*] and Nakhyun Chun [2]

[1] Seismic Research and Test Center, Pusan National University, 49, Busandaehak-ro, Yangsan 50612, Republic of Korea; bkjeon79@pusan.ac.kr (B.-G.J.); sjchang@pusan.ac.kr (S.-J.C.); swkim09@pusan.ac.kr (S.-W.K.)

[2] Structural & Constructional Technology, Group, KEPCO Research Institute, 105, Munji-ro, Yuseong-gu, Daejeon 34056, Republic of Korea; nhchun84@kepco.co.kr

* Correspondence: kwenry@pusan.ac.kr

Abstract: Among national infrastructure facilities, electric power facilities are very important sites that must maintain their functions properly even during a natural disaster or during social crises. Therefore, seismic design is required when necessary for major electric power facilities that have a significant impact when damaged in the event of an earthquake. In electric power facilities, bushings are generally installed in devices or structures. Therefore, ground acceleration can be amplified through devices, such as transformers, or sub-structures. Among various electric power facilities, cable terminations are representative cantilever-type substation facilities consisting of a bushing, a sub-structure, and support insulators. The bushings of cable terminations are generally made of porcelain or fiber-reinforced plastic (FRP) materials, and they may have different dynamic characteristics. This study attempted to estimate the acceleration amplification ratio in the main positions of cable terminations considering the materials of bushings. For two cable terminations with different specifications and bushing materials, three-axis shake table tests were conducted in accordance with IEEE 693, which includes a seismic performance evaluation method for a power substation facility. The acceleration amplification ratios at the top of the bushing, mass center, and top of the support structure were estimated using the acceleration responses of each cable termination. They were then compared with the acceleration amplification factors presented in design standards. Consequently, the acceleration amplification ratio of cable termination with an FRP bushing was lower than that of the cable termination with a porcelain bushing.

Keywords: seismic performance; electric power facility; bushing; amplification ratio; shaking table test; cable terminations

Citation: Jeon, B.-G.; Chang, S.-J.; Kim, S.-W.; Park, D.-U.; Chun, N. Experimental Study on the Acceleration Amplification Ratio of Cable Terminations for Electric Power Facilities. *Energies* **2024**, *17*, 5641. https://doi.org/10.3390/en17225641

Academic Editor: Juan-José González de la Rosa

Received: 7 October 2024
Revised: 31 October 2024
Accepted: 7 November 2024
Published: 11 November 2024

1. Introduction

Damage to several electric power facilities was reported during the Wenchuan earthquake (2008), Haiti earthquake (2010), and Tohoku earthquake (2011) [1–4]. Among the national infrastructure facilities, electric power facilities are essential facilities that must maintain their functions even during a natural disaster or a social crisis. The seismic safety of electric power facilities is even more important than anything else because the supply of electricity is vital in implementing rapid social stability and reconstruction projects after an earthquake. Therefore, establishing measures for seismic safety is required for major electric power facilities that have a significant impact when damaged in the event of an earthquake.

Since electric power facilities involve damage to themselves and socioeconomic impacts due to long-term power outages in the event of an earthquake, measures to prepare for earthquakes and secure seismic safety for electric power facilities need to be prepared. In this regard, applying a vibration control device such as a tuned mass damper (TMD) is

considered [5], and the seismic design or seismic qualification of electric power facilities is performed.

In general, seismic acceleration that acts on a structure or device is transmitted from the ground surface, and it increases as the height of the structure increases. The amplification factor easily applicable to seismic design is used as a design variable to reflect the influence of seismic acceleration that increases alongside the increase in height.

In ASCE 7-16, the amplification factor of a structure is linearly proportional to the total height of the structure and the installation height of the target facility. In addition, amplification factors were presented for various types of non-structural elements. Non-structural elements are divided into architectural components and mechanical/electrical components, while coefficients between 1 and 2.5 are presented [6]. The seismic design standards for buildings in Korea similarly present amplification factors to ASCE 7-16 [7]. These amplification factors of power transformer structures in Korea are applied in accordance with the guidelines on the seismic design of power transmission and distribution facilities [8]. The amplification factors of electric power facilities, however, are presented only for specific devices. For bushings, only the bushings of transformers are considered, and an amplification factor of 8.5 is used. In general, bushings are not mounted on the ground or simple support structures. Thus, the ground acceleration can be amplified through devices, such as transformers, or sub-structures. For this reason, IEEE 693 (2005) [9] applies four times the input seismic motion when the seismic performance of the bushings of transformers is evaluated through shake table tests. IEC TS 61463 presents the amplification factors of bushings considering devices and structures in which bushings are installed, the height, damping ratio, and multi-mode response [10]. Depending on the specifications or standards, the seismic acceleration amplification of electric power facilities can be considered differently.

Major electric power facilities are designed to be earthquake-resistant in accordance with design standards, and the validity of seismic design is evaluated through finite element analysis or experiments [9,11–13]. Bushings that are used in transformers, circuit breakers, gas-insulated switchgear (GIS), and cable terminations are representative electric power facilities whose seismic performance is evaluated through shake table tests. Shake table tests are mostly conducted on bushings because it is not economical to evaluate the seismic performance of large devices, such as transformers and liquid-filled reactors, through shake table tests.

Shake table tests were conducted to evaluate the seismic performance of large bushings over 500 kV [14,15]. In Korea, the seismic performance of various types of bushings was also evaluated [16,17]. For tests on bushings alone, however, it is difficult to consider interactions with devices or sub-structures on which bushings in transformers and GIS are mounted. Therefore, the seismic behavior of the entire device is analyzed, and its seismic performance is evaluated through finite element analysis considering the shake table test results of bushings [18,19]. Finite element analysis is conducted under the assumption that the device is ideally fixed to the floor. Such an ideal fixing, however, is not easy in the field. Thus, it is necessary to express the boundary conditions of the device accurately [20]. In addition, connections between the components of the device are complex. It is difficult to simulate them, as there are various variables [9]. Therefore, experimental studies aimed to analyze the seismic behavior of transformers and their bushings and investigate their acceleration amplification tendencies through shake table tests [21,22]. Recently, a study evaluated the seismic performance of a real-scale 154 kV transformer, which was equipped with all components (e.g., conservator and radiator) and filled with oil. The acceleration amplification ratio of the bushing was also analyzed [23].

Among various outdoor transformer facilities, cable terminations are a representative cantilever-type power substation facility that consists of a bushing, a sub-structure, and support insulators. They are used to connect overhead lines and underground lines at outdoor substations, and proper seismic design is required to maintain their functions in the event of an earthquake. Few studies, however, have been conducted on the seismic behavior and acceleration amplification tendency of cable terminations.

In the Seismic Research and Test Center of the Pusan National University, static tests and shake table tests were conducted on a 500 kV cable termination, which included a support structure, support insulators, and a fiber-reinforced plastic (FRP) bushing similar to those supplied [24]. Shake table tests and finite element analysis were also conducted to evaluate the seismic performance of a 230 kV cable termination [17]. In these studies, however, the seismic acceleration amplification of cable terminations was not analyzed. Therefore, if vibration amplification tendencies are investigated using the acceleration responses in major positions of the cable terminations among the shake table test data, it is expected that they can be used as data for determining the amplification factor for seismic design.

This research intended to estimate the acceleration amplification ratio in the main positions of cable terminations. For two cable terminations, three-axis shake table tests were conducted in accordance with IEEE 693 (2005) [9], which includes a seismic performance evaluation method for substation facilities. The resonant frequency was investigated from the tests, and the acceleration amplification ratios at the top of the bushing, mass center of the unit under tests, and on top of the support structure were estimated using the time history test results. Consequently, the acceleration amplification ratio of cable termination with an FRP bushing was lower than that of the cable termination with a porcelain bushing. In addition, the acceleration amplification ratio of the cable termination with an FRP bushing differed significantly from the design standard.

2. Earthquake Damage in Electric Power Facilities

Among electric power facilities, power transmission, and distribution facilities are major facilities that transmit electricity produced from power plants to each region that has demand for it. During the Wenchuan earthquake (2008), Haiti earthquake (2010), and Tohoku earthquake (2011), damage to a number of power transmission and distribution facilities was reported. Table 1 shows representative cases of seismic damage to power transmission and distribution facilities.

Circuit breakers, GIS, cable terminations, and cantilever-type slender bushings are installed in transformers. The structural vulnerability of bushings can be confirmed from a number of seismic damage cases. The 1985 Mexico City earthquake damaged the bushings of circuit breakers and transformers [25]. The 1989 Loma Prieta earthquake damaged the bushings of live tank breakers [26], while the 2003 Bam earthquake damaged the connecting joints of porcelain bushings [27]. Specifically, during the 2008 Wenchuan earthquake in China, damage to the bushings of transformers and circuit breakers was confirmed in a number of substations, including the Ertaishan and Qimingxing substations [1]. Damage to bushings was also reported during the Haiti and Chile earthquakes in 2010 [2,4]. Recently, during the 2023 Türkiye earthquake, damage to transformer bushings was reported from power plant facilities in the İskenderun and Elbistan regions [28]. Table 1 lists representative cases of seismic damage to substations and major facilities, while Figure 1 shows damage to bushings.

Seismic damage tends to be concentrated on bushings among the components of electric power facilities. Particularly, cable terminations can be vulnerable to seismic loads because they are slender and have a relatively high center of gravity since they consist of a bushing, support insulators, and a steel truss structure. Thus, the seismic safety of cable terminations is often verified through shake table tests. There are, however, few cases in which the seismic behavior of cable terminations was investigated through experiments. Therefore, in this study, shake table tests were conducted to analyze the seismic acceleration amplification tendency of cable terminations.

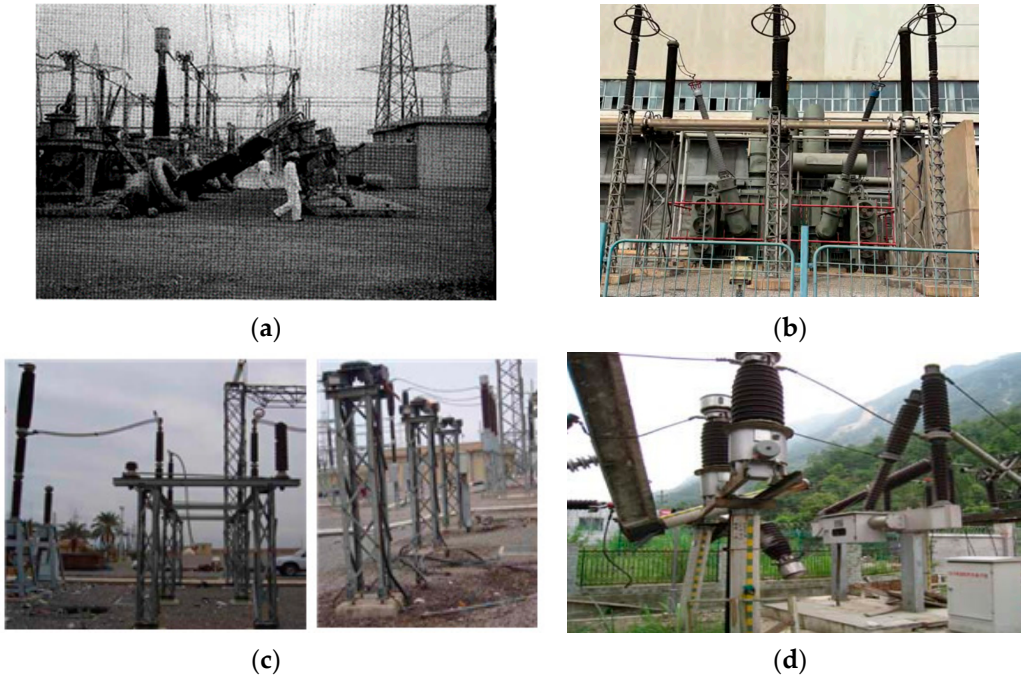

Figure 1. Seismic damage to bushings in substations: (**a**) overturned 500 kV circuit breaker at the Moss Landing substation [29]; (**b**) sustained broken bushing [28]; (**c**) Bam city earthquake (2004) [27]; (**d**) Wenchuan earthquake [1].

Table 1. Cases of seismic damage to electric power facilities.

Country (Year)	Location	Damage	Failure Mode
Mexico (1985)	Yautepec substation	• power transformer bushings • surge arresters (ground-mounted) • instrument transformers • circuit breakers (live tank)	• overturning by anchorage failure • knocking building
	Oaxaca substation	• transformer	• overturning by anchorage failure
The U.S. (Loma prieta) (1989)	Moss Landing substation	• live tank breakers bushing • instrument transformer	• overturning broken by bending
Iran (2003)	substation in Tehran and Tabriz	• insulator and bushing • transformers • CVTs and CTs • batteries in the control building	• overturning by anchorage failure • impact by pendulous motions of LTs • fall down
China (2008)	more than 100 substations including Ertaishan substation	• transformer • switchgear • cores/coils • bushings • radiators • conservators	• sliding • dropping • overturning • tippling • rupture • oil leakage
Haiti (2010)	Ancien Delmas substation and Nouveau Delmas substation [30]	• transformer	• overturning • oil leakage • broken insulators
Chile (2010)	substation near Quillota	• inclined isolators • current and measuring transformers	• oil leakage • slant
Türkiye (2023)	İskenderun, Elbistan and antakya area [28]	• transformer movement • oil leakage • broken bushings • settlement of powerhouse • collapse of substation buildings • collapse of transmission tower	

3. Unit Under Tests

The units under test (UUTs) were cable terminations designed and produced by different manufacturers. UUT1 is a 500 kV cable termination that consists of an FRP bushing, eight porcelain support insulators, and a truss-type steel support structure. It measures 9253 mm in height and weighs 4900 kg. UUT2 is a 230 kV cable termination that consists of a porcelain bushing, four porcelain support insulators, and a steel support structure. It measures 6000 mm high and weighs 2108 kg. The bushings of the UUTs were filled with insulating oil and additional mass that serves as conductors, and cables were installed at terminal connections [9]. The UUTs had cables with a sufficient length for function tests. Figure 2 and Table 2 show the geometry and details of the UUTs. The support structure of UUT1 was fastened with a steel jig, which was fixed to the floor of the shake table using M30 bolts (Torque: 770 N·m). The end of the cable was also fixed to the floor of the shake table using a fixing tool.

Table 2. Specification of UUTs.

Specimen Name	Specification	Dimensions (mm)			Weight (kg)	Added Weight (kg)
		Length	Width	Height		
UUT1	500 kV	2348	1219	9253	4900	12.62
UUT2	230 kV	1212	1212	6000	2108	7.10

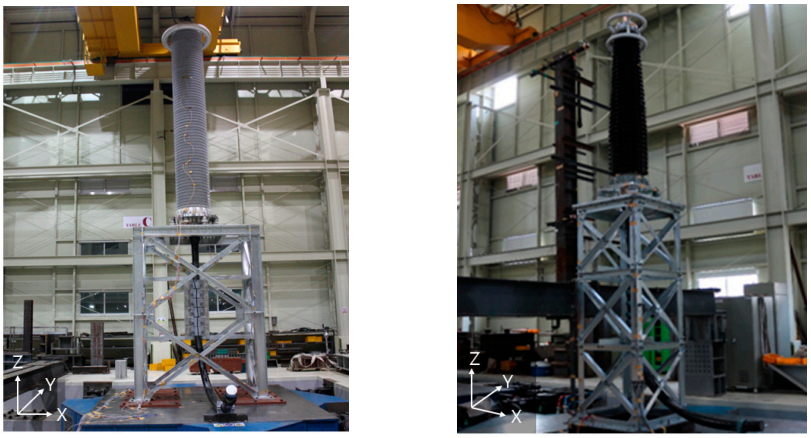

(**a**) (**b**)

Figure 2. UUTs on shaking table: (**a**) UUT1, 500 kV cable termination; (**b**) UUT2, 230 kV cable termination.

4. Shaking Table Tests

This study performed shake table tests in accordance with IEEE 693 (2005), which is a test standard for examining the seismic design of substation facilities. Table 3 shows the sequence of the tests.

Table 3. Test procedure.

Step	Test Name
1	pre-resonance search test
2	Time history test
3	post-resonance search test

4.1. Resonance Search Test

The resonance search test is conducted to find the resonant frequency and the damping ratio. In this study, the UUTs were installed on the shake table, as reflected in Figure 2, and a resonance search was performed by conducting the sine sweep test. The test was conducted in both vertical and horizontal directions. Since the target facilities were flexible structures with a high center of gravity, the resonance search test was conducted using low input acceleration (0.05 g) so that the structures would not be damaged. The search range was set at 1 to 35 Hz.

4.2. Time History Test

For the time history test, acceleration time history was prepared to satisfy the high-level required response spectrum (RRS) for the 2% damping ratio proposed by IEEE 693 (2005) [9]. Figure 3a shows the horizontal RRS, and Figure 3b demonstrates the vertical RRS. For the vertical direction, 80% of the horizontal component was used in accordance with IEEE 693 (2005) [9]. A tri-axial test was conducted using the prepared artificial seismic wave. The artificial seismic wave vibration lasted 30 s, and that of strong motion was 20 s [31]. The tri-axial test means that both horizontal and vertical directions are tested simultaneously. Figure 4 depicts that the RRS is well enclosed in the tested response spectrum (TRS) of the acceleration signal measured on the floor of the shake table. In Figure 4, the left side shows the acceleration response in each axis, while the right side compares the TRS and RRS. The RRS is represented by black lines, and the TRS is represented by red lines. Lines that correspond to 90% and 150% of the RRS were expressed using blue dotted lines. The blue dotted lines are the tolerance of table motion recommended by IEEE 693 (2005) [9].

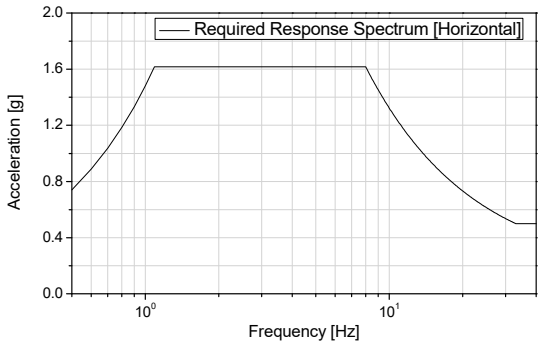

(**a**)

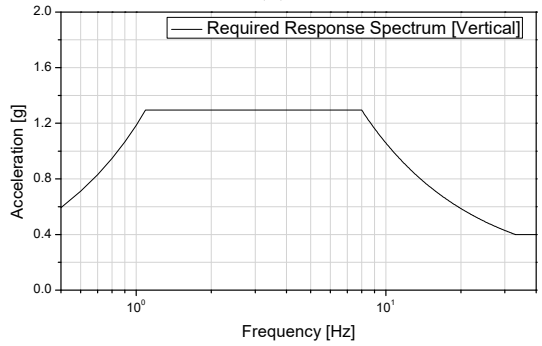

(**b**)

Figure 3. Required response spectrum (2% damping ratio): (**a**) horizontal; (**b**) vertical.

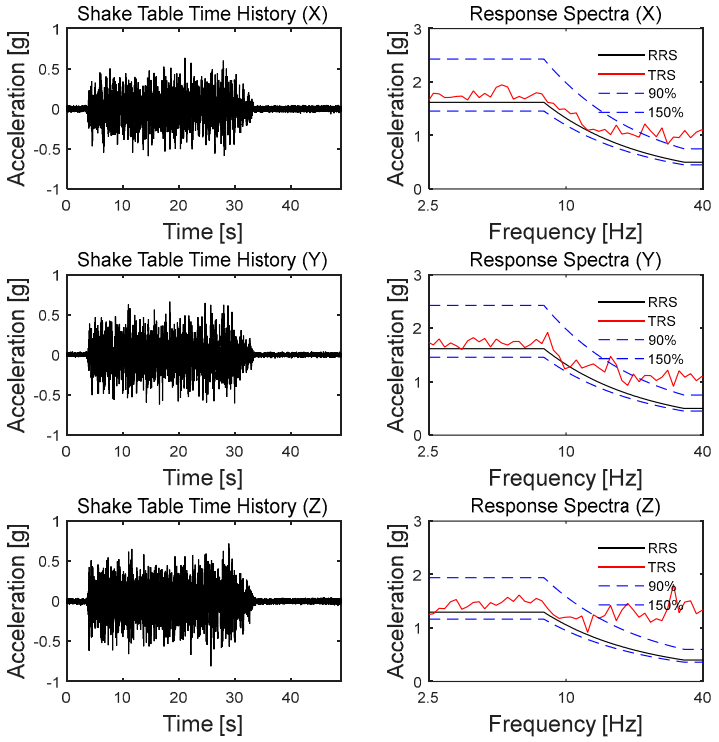

(**a**)

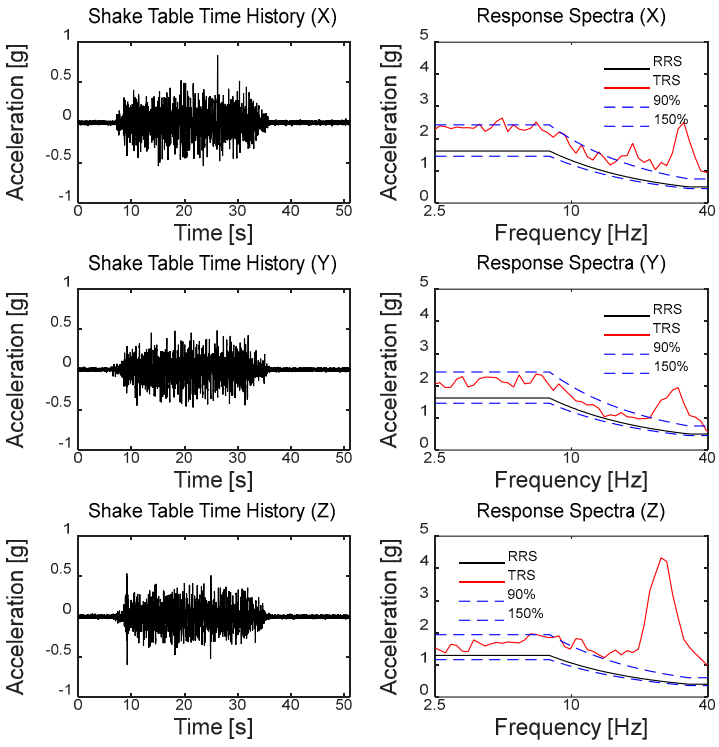

(**b**)

Figure 4. Time history of input acceleration (left) and comparison between TRS and RRS (right): (**a**) UUT1 500 kV cable termination; (**b**) UUT2 230 kV cable termination.

5. Test Equipment and Measurement

5.1. Test Equipment

Shake table tests were conducted using the six-degrees-of-freedom (6DOF) shake table of the Seismic Research and Test Center of Pusan National University. The maximum load of the shake table is 30 tons, and the maximum acceleration for a bare table is 3.0 g. Figure 5 and Table 4 show pictures and performance details of the 6DOF shaking table.

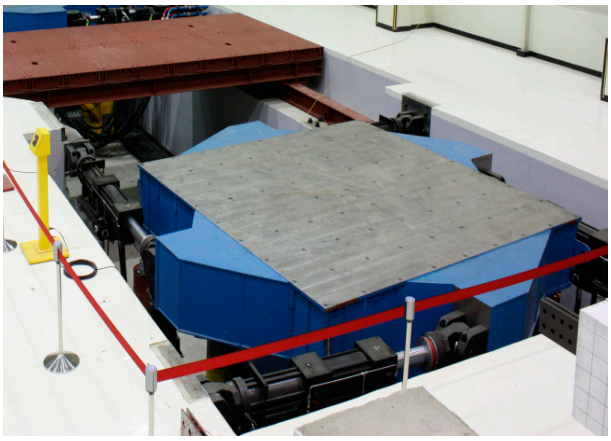

Figure 5. The 6DOF shaking table at SESTEC.

Table 4. The 6DOF shaking table at SESTEC.

Item	Specification
degrees of freedom	6DOF
table size	4 m × 4 m
full payload	30 tons
maximum acceleration (bar table)	3.0 g
maximum velocity	150 cm/s
maximum stroke	±30.0 cm (±20.0 cm)

5.2. Measurement

To measure test responses, accelerometers were installed in major positions. The accelerometer installation positions are highlighted in Figure 6. The yellow triangles mean locations for accelerometers.

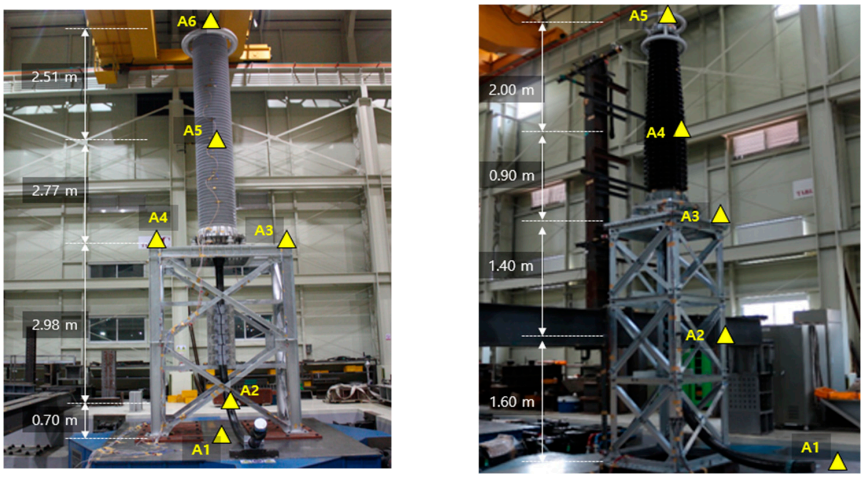

(**a**) (**b**)

Figure 6. Tri-axial accelerometer location: (**a**) UUT1; (**b**) UUT2.

As for the accelerometers, tri-axial accelerometers were used to measure acceleration responses in two horizontal directions and one vertical direction in the same position. Accelerometers were installed on the shake table to examine the control results of the shake table tests. To measure the acceleration responses of the target facilities, tri-axial accelerometers were installed at the top of the bushing, at the mass center, and on top of the support structure.

6. Test Results and Analysis

Upon completing the test, structural abnormalities such as cracks, leakage, and loosened bolts were examined, and function tests were conducted at the manufacturer's site. No structural damage was found for both UUT1 and UUT2, and their main functions were normal.

6.1. Estimation of the Resonant Frequency and Damping Ratio

The resonant frequencies of the target facilities were determined by calculating the transfer function through the resonance search test. The transfer function was obtained by calculating the acceleration (Unit, $b(t)$) at the response position with respect to the input acceleration (Base, $a(t)$) using Equation (1). A Symmetric Hamming Window was applied to each signal to prevent signal distortion in the frequency domain.

$$T_{ab}(f) = \frac{P_{ba}(f)}{P_{ba}(f)} \tag{1}$$

where $T_{ab}(f)$ is the transfer function of the output acceleration signal ($b(t)$) with respect to the input acceleration signal ($a(t)$), $P_{aa}(f)$ is the Power Spectral Density function of the input signal, and $P_{ba}(f)$ is the Cross-Power Spectral Density function of the input and output signals.

This study estimated the damping ratio using the half-power bandwidth method, which is most commonly used to estimate the damping ratio through shake table tests. The half-power bandwidth method estimates the damping ratio using the target half-power bandwidth frequency in the frequency domain of the measured acceleration signal. The half-power bandwidth frequency (β_1, β_2) can be defined for the damping ratio (ξ), as noted in Equation (2). In Equation (2), β_n^2 is the natural frequency of an equivalent vibration system. In terms of ξ, the damping ratio of the target mode can be estimated using Equation (3) in the case of low damping.

$$\beta_1^2,\ \beta_2^2 = \left[\left(1 - 2\xi^2\right) \mp 2\xi\sqrt{1 - \xi^2}\right]\beta_n^2 \tag{2}$$

$$\xi = (\beta_2 - \beta_1)/(\beta_2 + \beta_1) \tag{3}$$

Table 5 shows the resonant frequency and damping ratio [32,33]. For UUT1 with an FRP bushing, the lowest resonant frequency estimated from the resonance search results before the test was 5.0 Hz for the *X*-axis, 4.5 Hz for the *Y*-axis, and 24.25 Hz for the *Z*-axis. Changes in resonant frequency after the test were insignificant. For UUT2 with a porcelain bushing, the resonant frequency before the test was 7.19 Hz for the *X*-axis, 7.13 Hz for the *Y*-axis, and 36.75 Hz for the *Z*-axis. Changes in resonant frequency before and after the test were less than 5%. The damping ratio of UUT1 is higher than that of UUT2. The average horizontal damping ratio of UUT1 was the same (5.81%) before and after the test, while that of UUT2 was 3.61% before the test and 3.81% after the test, resulting in a difference of less than 5%. For both UUT1 and UUT2, the resonant frequency and damping ratio changed by less than 5%, indicating that no structural damage occurred.

Table 5. Resonant frequency and damping ratio.

Test Name	Direction	Lowest Resonant Frequency (Hz)		Damping Ratio (%)		Remarks
		UUT1	UUT2	UUT1	UUT2	
pre-resonance search test	X	5.00	7.19	5.56	3.26	half-power bandwidth
	Y	4.50	7.13	6.06	3.95	
	Z	24.25	36.75	1.90	1.62	
post-resonance search test	X	5.00	7.00	5.56	4.02	
	Y	4.50	6.94	6.06	3.60	
	Z	24.50	34.94	1.37	1.34	

6.2. Acceleration Amplification Ratio

For equipment with various components, a comparison that uses the maximum value of the acceleration response may not be appropriate due to the influence of the local mode and the noise caused by interactions between the components. In NUREG/CR-5203, the acceleration amplification ratio of cabinets, among electrical devices, is presented using the average value, peak value, or the value of the zero period in the random frequency range of the acceleration response spectrum [34]. Therefore, the acceleration amplification tendency was analyzed using the ZPA of the test acceleration response spectrum and RMS (Root Mean Square) of the time history as representative values. The test acceleration response spectrum was analyzed using a 1/12 octave.

In Table 5, ZPA represents the spectral acceleration values at the TRS of 47.95 Hz for the acceleration responses measured from the accelerators. In IEEE 693 (2018) [35], the ZPA in shake table tests is an acceleration value in a high-frequency domain of 33 Hz and up, and it indicates the maximum acceleration value of the acceleration time history. Here, it appears that 33 Hz was mentioned because the range of RRS presented for creating the acceleration time history is 33 Hz or less. Therefore, the highest frequency value of RRS or the frequency operating limit of the shake table can be used by assuming them as zero periods [23]. In this study, the spectral acceleration value at the TRS of 47.95 Hz measured from each accelerometer was assumed to be the ZPA, considering the frequency range of the shake table and the TRS octave.

The acceleration amplification tendencies of the UUTs were compared using the ratio between the acceleration response at the main positions and the acceleration response of the shake table floor. The ratio of the acceleration response spectrum, $R_a(i)$, can be calculated using Equation (4). In Equation (4), $S_a(Ground)$ is the TRS of the acceleration response measured at the top of the concrete foundation installed on the shake table, and $S_a(Component)$ is the FRS measured from each position of the test target. i is the measurement position. $R_a(i)$ is shown in Table 6.

$$R_a(i) = \frac{S_a(Floor)}{S_a(Ground)} \tag{4}$$

The RMS can be used to evaluate the acceleration response of electrical equipment [36]. The RMS of the time history is the square root value of the average of the squares of the time history measured at each position. It can be seen as a value that represents the amplitude regardless of the frequency, which can be expressed as Equation (5).

$$\text{RMS} = \sqrt{\frac{1}{n}\sum_{k=1}^{n} x_k^2} \tag{5}$$

where x_k is the k-th data in the measured time history, and n is the total number of time history data. Since RMS, which is calculated based on the signals measured at each position,

represents the amplitude of the positions, the RMS ratio can be calculated using Equation (6) in the same way as the acceleration response spectrum ratio shown in Equation (4).

$$R_{RMS}(i) = \frac{RMS_a(Floor)}{RMS_a(Ground)} \tag{6}$$

where RMS_a (*Component*) is the RMS value of the acceleration time history measured at the main positions of the test target, $RMS_a(Ground)$ is the RMS value of the acceleration time history measured at the base of the shake table, and i is the measurement position. Table 7 specifies the RMS values and RMS ratios for tri-axial acceleration in the main positions of the UUTs.

Table 6. The ZPA (47.95 Hz) and $R_a(i)$.

Location	Direction	ZPA (g)		$R_a(i)$ (g/g)	
		UUT1	UUT2	UUT1	UUT2
shaking table	X	1.28	0.86	-	-
	Y	1.59	0.56	-	-
	Z	1.97	0.92	-	-
top of sub-structure	X	0.95	2.16	0.74	2.51
	Y	1.07	1.94	0.67	3.46
	Z	0.80	1.32	0.41	1.44
mass center of UUT	X	1.21	2.13	0.96	2.48
	Y	1.21	2.14	0.76	3.82
	Z	0.58	2.29	0.29	2.49
top of UUT	X	2.34	4.88	1.83	5.67
	Y	2.35	4.34	1.48	7.75
	Z	0.96	2.67	0.49	2.90

Table 7. RMS and $R_{RMS}(i)$.

Location	Direction	RMS of Acceleration (g)		$R_{RMS}(i)$ (g/g)	
		UUT1	UUT2	UUT1	UUT2
shaking table	X	0.12	0.12	-	-
	Y	0.13	0.11	-	-
	Z	0.12	0.10	-	-
top of sub-structure	X	0.13	0.25	1.08	2.08
	Y	0.15	0.24	1.15	2.18
	Z	0.14	0.13	1.17	1.30
mass center of UUT	X	0.23	0.46	1.92	3.83
	Y	0.26	0.43	2.00	3.91
	Z	0.10	0.14	0.83	1.40
top of UUT	X	0.48	0.74	4.00	6.17
	Y	0.51	0.73	3.92	6.64
	Z	0.11	0.15	0.92	1.50

Figure 7 shows the amplification ratios of the acceleration response of each axis to the input earthquake for UUT1 and UUT2 according to the measurement height. Figure 7a shows the amplification ratio of UUT 1 and that of UUT2 in Figure 7b.

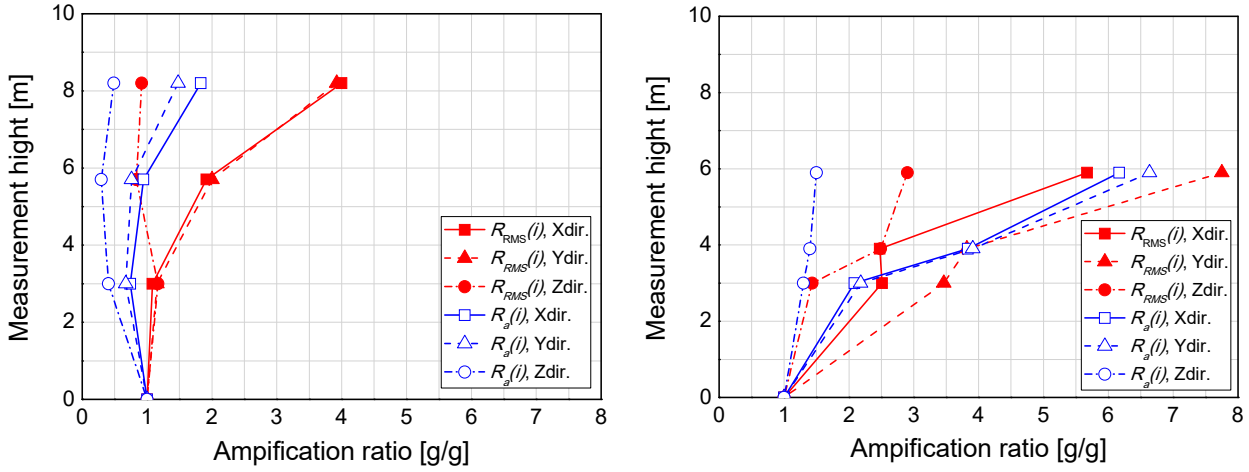

Figure 7. Comparison of amplification ratios: (**a**) amplification ratio of UUT1; (**b**) amplification ratio of UUT2.

In Figure 7, $R_a(i)$ is marked by blue lines and $R_{RMS}(i)$ by red lines. Solid lines, dot lines, and dash–dot lines represent the X-direction, Y-direction, and Z-direction acceleration amplification ratios, respectively. In Figure 7a, for $R_a(i)$ of UUT1, all values in the top horizontal direction are less than 1 as they range from 0.294 to 0.945. $R_{RMS}(i)$ is higher than 1 at all positions except for the Z-direction of UUT1. In particular, $R_{RMS}(i)$ is 3.9 or higher in the top horizontal direction. $R_{RMS}(i)$ in the Z-direction of UUT1, however, is less than 1 at height above the center of gravity.

In Figure 7b, both $R_a(i)$ and $R_{RMS}(i)$ of UUT2 are higher than 1. There is a difference in the acceleration amplification tendency of the Z-axis. In the horizontal direction, however, the value of the acceleration amplification ratio increased similarly as the height of the acceleration response measurement position increased. For the acceleration amplification ratio of the mass center, $R_a(i)$ and $R_{RMS}(i)$ were more than twice as different for UUT1, and a difference of 1.5 times was also confirmed in the X-direction of UUT2. The amplification factor can be calculated using various factors depending on its definition, but the difference can be significant or the tendency can vary depending on the calculation method.

Table 8 summarizes the acceleration amplification ratios of the top of the bushing and the mass center. The differences in $R_a(i)$ for the two different horizontal directions of UUT1 and UUT2 are 9.93 and 31.83% at the top of the structure, 23.26 and 42.54% at the mass center of the UUTs, and 21.15 and 31.00% at the top of the UUTs. In the case of $R_{RMS}(i)$, however, the maximum error between the X-axis and Y-axis of UUT1 and UUT2 at all positions is less than 7.34%, which is not significant compared to $R_a(i)$. In Table 4, the lowest resonant frequencies in the horizontal direction for UUT1 and UUT2 are 4.5 and 7.13 Hz, respectively. Hence, to obtain the acceleration amplification ratio of cantilever-type structures that do not have a high resonant frequency, such as terminations, it is deemed reasonable to use the RMS value of the response acceleration time history as a representative value rather than using the ZPA value of the test acceleration response spectrum.

$$\text{Difference } (\%) = \frac{|E_1 - E_2|}{1/2(E_1 + E_2)} \times 100 \tag{7}$$

Figure 8 displays the amplification ratios of the mass center of the UUTs. Figure 9 details the amplification ratios of the top of the UUTs.

Table 8. Amplification ratios of cable terminations.

Location	Direction		$R_a(i)$ (g/g)		$R_{RMS}(i)$ (g/g)	
			UUT1	UUT2	UUT1	UUT2
top of the support structure	amplification ratio (g/g)	X	0.74	2.51	1.08	2.08
		Y	0.67	3.46	1.15	2.18
		average	0.71	2.99	1.12	2.13
	difference (%)		9.93	31.83	6.28	4.69
mass center of UUT	amplification ratio (g/g)	X	0.96	2.48	1.92	3.83
		Y	0.76	3.82	2.00	3.91
		average	0.86	3.15	1.96	3.87
	difference (%)		23.26	42.54	4.08	2.07
top of UUT	amplification ratio (g/g)	X	1.83	5.67	4.00	6.17
		Y	1.48	7.75	3.92	6.64
		average	1.66	6.71	3.96	6.41
	difference (%)		21.15	31.00	2.02	7.34

The amplification factor of transformer bushings in Korean electric power facilities is 8.5 [8], while the maximum acceleration amplification factor of transformer bushings in IEC TS 61,463 is 9.6 [10,23]. In Figure 9, the maximum $R_a(i)$ of UUT2 is 7.75 and the maximum $R_{RMS}(i)$ is 6.64 or less, which is smaller than the amplification factor of transformer bushings in Korean electric power facilities (8.5), and the differences are 9.23 and 24.57%, respectively. In the case of UUT1 with a flexible FRP bushing, however, $R_a(i)$ is 1.83 or less and $R_{RMS}(i)$ is 4.00 or less, which is very low compared to 8.5. Thus, very low values compared to the amplification factor presented by the seismic qualification specification of bushings can be seen in Figure 9. It must be considered, however, that the acceleration amplification factors compared with the test results are only for transformer bushings.

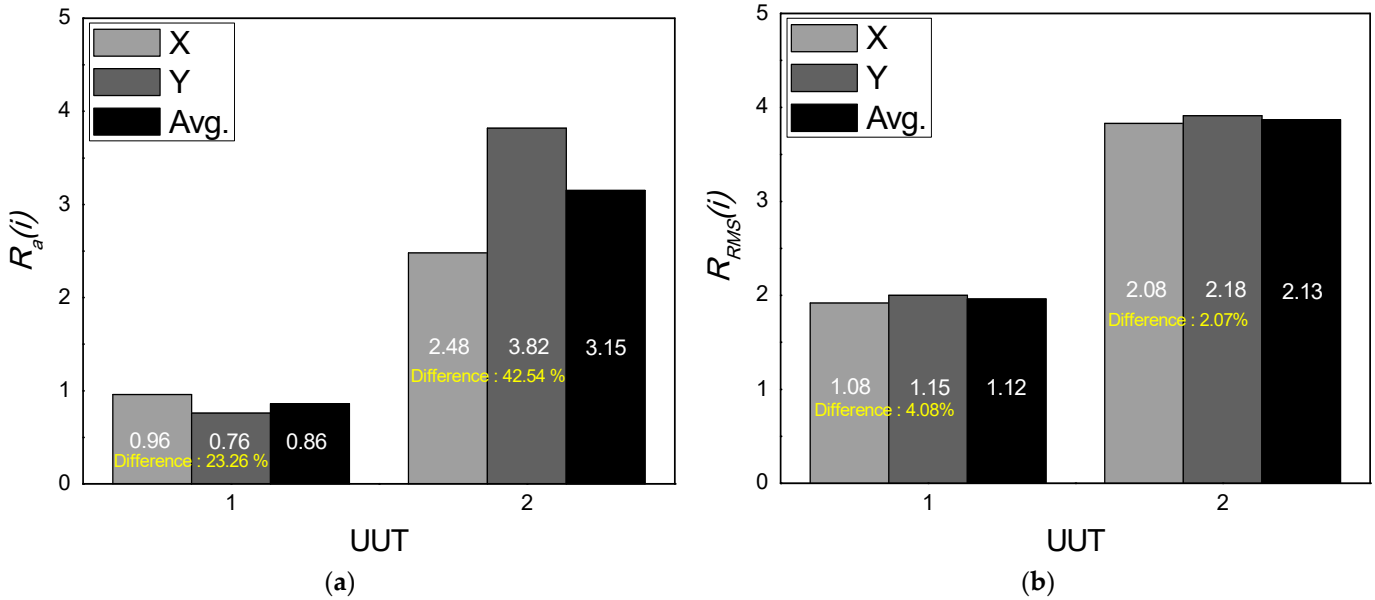

Figure 8. Amplification ratios of the mass center of UUTs: (**a**) $R_a(i)$ of mass center of UUTs; (**b**) $R_{RMS}(i)$ of mass center of UUTs.

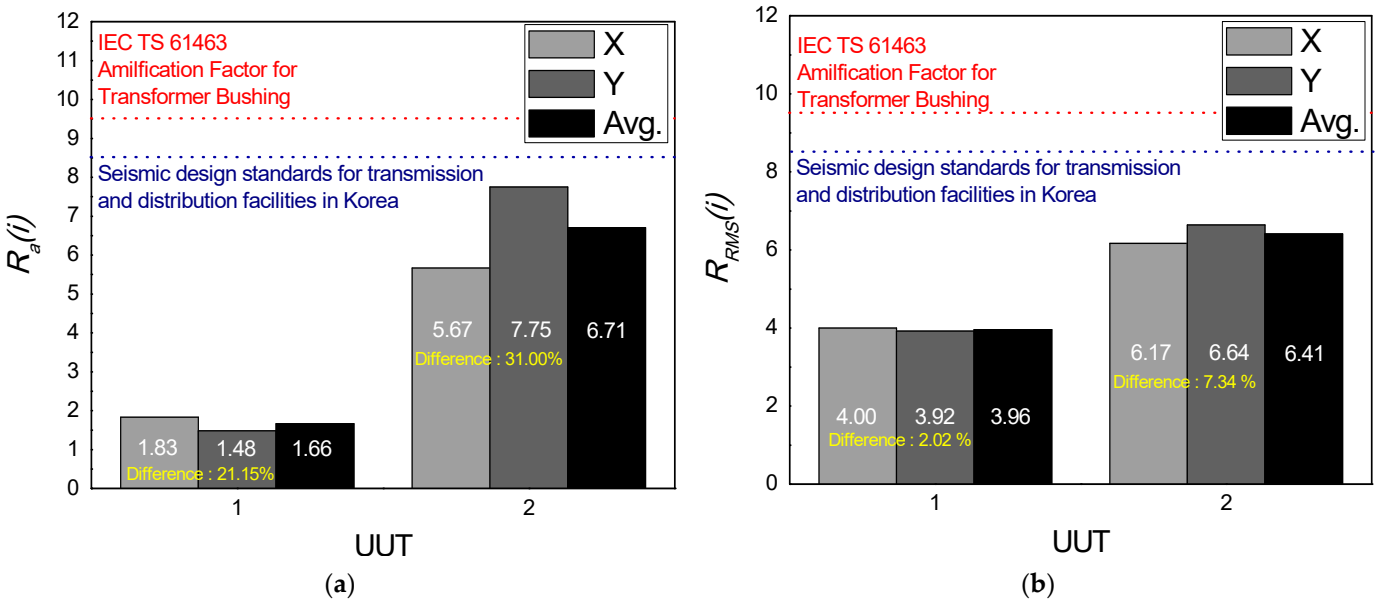

Figure 9. Amplification ratios of top of UUT: (**a**) $R_a(i)$ of top of UUTs; (**b**) $R_{RMS}(i)$ of top of UUTs.

In IEEE 693, most support structures are verified using the modified input operation conservatively allowed. In D.5 (Qualification procedures for bushings) of IEEE 693 (2018) [35], transformer bushings must be tested twice using RRS to consider amplification by the transformer. In addition, in IEEE 693 (2018) [35] 5.10.4, testing must be conducted using 2.5 times RRS when the parameters of a support structure are not known. In other words, IEEE 693 (2018) [35] considers 2 to 2.5 times the amplification of seismic force by the sub-structure or device of bushings.

Table 9 lists the acceleration amplification ratios at the top of the sub-structure for UUT1 and UUT2 analyzed through $R_a(i)$ and $R_{RMS}(i)$. Figure 10 presents the X-direction, Y-direction, and average values for $R_a(i)$ and $R_{RMS}(i)$.

Table 9. Amplification ratio at the top of the support structure of cable terminations.

Direction		$R_a(i)$ (g/g)		$R_{RMS}(i)$ (g/g)		IEEE 693 Maximum Amplification Ratio of Support Structure
		UUT1	UUT2	UUT1	UUT2	
horizontal	X	0.74	2.51	1.08	2.08	2.50
	Y	0.67	3.46	1.15	2.18	
vertical	Z	0.41	1.44	1.17	1.30	

In Figure 10a, the acceleration amplification ratio in the horizontal direction at the top of the sub-structure of UUT2 is 2.51 for the *X*-axis, 3.46 for the *Y*-axis, and 2.99 on average for $R_a(i)$. Therefore, the difference from the amplification factor of sub-structures presented by IEEE (2.5) is up to 32.22%, while the average value showed a difference of 17.85%. When the acceleration amplification ratio was calculated using $R_{RMS}(i)$, as indicated in Figure 10b, the values are 2.08 for the *X*-axis and 2.18 for the *Y*-axis. Since the average is 2.13, its difference from the amplification factor (2.5) of IEEE 693 (2018) [35] is less than 16%. Unlike UUT2, however, $R_a(i)$ and $R_{RMS}(i)$ of UUT1 were significantly lower than 2.5 in all directions.

The *Z*-axis (vertical) acceleration amplification ratios of UUT1 and UUT2 are lower than 1.44 for both $R_a(i)$ and $R_{RMS}(i)$. Therefore, the vertical acceleration amplification ratios of the UUTs are significantly low compared to IEEE 693 (2018) [35].

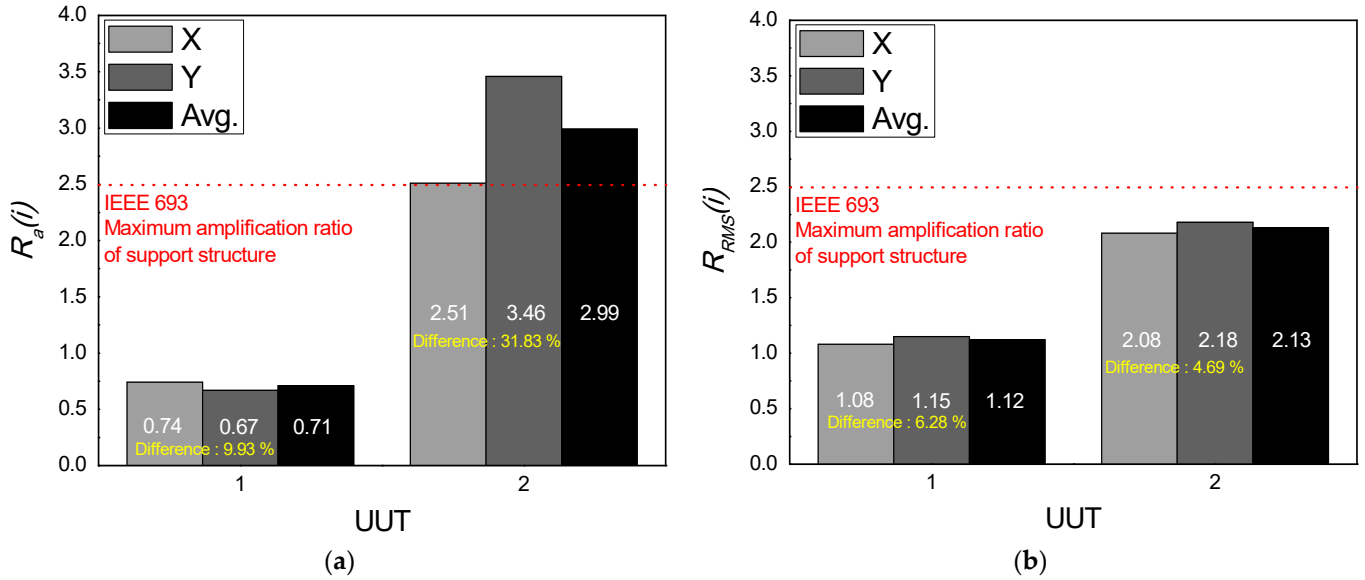

Figure 10. Amplification ratio considering the support structure for terminations: (**a**) $R_a(i)$ of top of support structures; (**b**) $R_{RMS}(i)$ of top of support structures.

7. Concluding Remarks

This study conducted three-axis shake table tests on two different cable terminations in accordance with IEEE 693 (2005) [9], which is a seismic performance evaluation method for substation facilities. Acceleration amplification tendencies at the main positions of the terminations under seismic loads were analyzed using response acceleration signals. The units under test (UUTs) involved a 500 kV termination with a fiber-reinforced plastic (FRP) bushing (UUT1) and a 230 kV termination with a porcelain bushing (UUT2).

The acceleration amplification ratio was calculated using $R_a(i)$ based on the ZPA of the tested response spectrum (TRS) and $R_{RMS}(i)$ that used the RMS value of the response acceleration time history. The acceleration amplification ratio of UUT1 with a low resonant frequency was lower than that of UUT2 with a high resonant frequency.

The difference in the acceleration amplification ratio of two different horizontal directions at the mass center and top of the UUTs was lower compared to when evaluated using $R_{RMS}(i)$ and $R_a(i)$. The difference in $R_a(i)$ ranged from 21.15% to 42.54%. The difference in $R_{RMS}(i)$, however, was smaller than 7.34%. Based on these test results, $R_{RMS}(i)$ that used the RMS value of the response acceleration time history as a representative value is judged to be more reasonable than $R_a(i)$ when compared using the ZPA value for obtaining the acceleration amplification ratio of a termination, which is a cantilever-type structure whose resonant frequency is not high.

There are limited data on the acceleration amplification factor of bushings in terminations under seismic loads. Therefore, a direct comparison is difficult, but a comparison was made with the amplification factors of transformer bushings. When the lower value (8.5) between the amplification factor of transformer bushings in Korean electric power facilities (8.5) and the acceleration amplification factor of transformer bushings in IEC TS 61463 (9.6) was compared with the experiment results, $R_a(i)$ was 80.47% lower and $R_{RMS}(i)$ was 53.41% lower for UUT1, while $R_a(i)$ was 21.06% lower and $R_{RMS}(i)$ was 24.59% lower for UUT2. In IEEE 693, the RRS is amplified by up to 2.5 times, considering the sub-structure of terminations. The acceleration response amplification ratios at the top of the sub-structure of the terminations obtained from the experiment results were compared with the amplification factor by sub-structures presented by IEEE 693. For UUT2 with a porcelain bushing, the average acceleration amplification ratio in the horizontal direction was 17.85% higher than the amplification factor of IEEE 693 (2.5) for $R_a(i)$ and 16.98% lower for $R_{RMS}(i)$. The acceleration amplification ratio by the sub-structure of UUT1 with a flexible FRP bushing, however, was significantly lower than 2.5 for both $R_a(i)$ and $R_{RMS}(i)$. The experiment

results confirm that the acceleration amplification ratio of UUT2 was not significantly different from the amplification factors presented by design standards or performance verification standards. The acceleration amplification ratio of UUT1 with an FRP bushing, however, was significantly different from the amplification factors presented by design standards or performance verification standards for both the bushing and sub-structure. As such, the acceleration amplification ratio of UUT2 with a porcelain bushing is less than 25% different from the design standard, but the acceleration amplification ratio of UUT 1 with an FRP bushing is more than 53% different from the design standard. Note that this result only considered the horizontal acceleration amplification.

The study's findings are expected to serve as foundational data for seismic design and seismic performance verification in securing the seismic safety of terminations among electric power facilities, which are classified as national infrastructure facilities.

Author Contributions: Conceptualization, B.-G.J. and N.C.; experimental tests, S.-J.C., S.-W.K. and D.-U.P.; methodology, S.-W.K., S.-J.C. and B.-G.J.; validation, D.-U.P. and N.C.; visualization, B.-G.J. and S.-J.C.; investigation, S.-W.K. and B.-G.J.; writing—original draft, B.-G.J.; writing—review and editing, B.-G.J., D.-U.P., S.-J.C. and N.C. All authors have read and agreed to the published version of the manuscript.

Funding: This work was supported by the Korea Institute of Energy Technology Evaluation and Planning (KETEP) and the Ministry of Trade, Industry & Energy (MOTIE) of the Republic of Korea (No. 20224B10200080).

Data Availability Statement: The original contributions presented in the study are included in the article, further inquiries can be directed to the corresponding author.

Acknowledgments: Special thanks to the Seismic Research and Test Center at Pusan National University for their valuable assistance during the testing process.

Conflicts of Interest: Author Nakhyun Chun was employed by the company Structural & Constructional Technology, Group, KEPCO Research Institute. The remaining authors declare that the research was conducted in the absence of any commercial or financial relationships that could be construed as a potential conflict of interest.

References

1. Liu, R.; Zhang, M.; Wu, L. Vulnerability Study of Electric Power Grid in Different Intensity Area in Wenchuan Earthquake. In Proceedings of the 15th World Conference of Earthquake Engineering (WCEE), Lisbon, Portugal, 24–28 September 2012.
2. Cruz, E.F.; Valdivia, D. Performance of industrial facilities in the Chilean earthquake of 27 February 2010. *Struct. Des. Tall Spec. Build.* **2011**, *20*, 83–101. [CrossRef]
3. Xue, Y.; Cheng, Y.; Zhu, Z.; Li, S.; Liu, Z.; Guo, H.; Zhang, S. Study on seismic performance of porcelain pillar electrical equipment based on nonlinear dynamic theory. *Adv. Civ. Eng.* **2021**, *2021*, 8816322. [CrossRef]
4. Fujisaki, E.; Takhirov, S.; Xie, Q.; Mosalam, K.M. Seismic Vulnerability of Power Supply: Lessons Learned from Recent Earthquakes and Future Horizons of Research. In Proceedings of the 9th International Conference on Structural Dynamics (EURODYN 2014), Porto, Portugal, 30 June–2 July 2014.
5. Wang, L.; Shi, W.; Li, X.; Zhang, Q.; Zhou, Y. An adaptive-passive retuning device for a pendulum tuned mass damper considering mass uncertainty and optimum frequency. *Struct. Control Health Monit.* **2019**, *26*, 2377. [CrossRef]
6. *ACSE/SEI 7-16*; Minimum Design Loads for Buildings and Other Structures. ASCE: Reston, VA, USA, 2017.
7. *KDS 41 17 00*; Seismic Design Code for Buildings. MOLIT: Sejong, Republic of Korea, 2019.
8. Korea Electric Power Cooperation (KEPCO). *Earthquake Resistant Design Guidelines of Transmission, Substation and Distribution Facilities*; KEPCO: Naju, Republic of Korea, 2019.
9. *IEEE 693-2005*; Recommended Practice for Seismic Design of Substations. IEEE: Piscataway, NJ, USA, 2005.
10. *IEC TS 61463*; Technical Specification. IEC: Geneva, Switzerland, 2016.
11. *IEC 62271-207*; High-Voltage Switchgear and Controlgear—Part 207: Seismic Qualification for Gas-Insulated Switchgear Assemblies for Rated Voltages Above 52kV. IEC: Geneva, Switzerland, 2007.
12. *IEC 62271-210*; Seismic Qualification for Metal Enclosed and Solid-Insulation Enclosed Switchgear and Controlgear Assemblies for Rated Voltages Above 1 kV and up to and Including 52 kV. IEC: Geneva, Switzerland, 2013.
13. *IEC 60068 3-3*; Environmental Testing—Part 3: Guidance—Seismic Test Methods for Equipments. IEC: Geneva, Switzerland, 1991.
14. Koliou, M.; Filiatrault, A.; Reinhorn, A.M.; Oliveto, N. *Seismic Protection of Electrical Transformer Bushing System by Stiffening Techniques: Technical Report MCEER-12-0002*; Multidisciplinary Center for Earthquake Engineering Research: New York, NY, USA, 2012.

15. Amir, S.G.; Whittaker, A.S.; Fenves, G.L.; Fujisaki, E. *Seismic Evaluation of 550 kV Porcelain Transformer Bearings: PEER Report 1999/05*; Pacific Earthquake Engineering Research Center: Richmond, CA, USA, 1999.
16. Joe, Y.H.; Cho, S.G. Modal identification and seismic performance evaluation of 154kV transformer porcelain bushing by vibration test. *J. Earthq. Eng. Soc. Korea* **2006**, *10*, 107–115.
17. Kim, S.W.; Park, D.U.; Jeon, B.G.; Yun, D.W. Response of a 230 kV outdoor termination according to the frequency characteristics of input seismic waves. *Energy Rep.* **2020**, *6*, 497–503. [CrossRef]
18. Ullah, K.N.; Mohammmad, A.S. *Electrical and Seismic Design of Electric Supply Substation*; LAP Lambert Academic Publishing: Saarbrucken, Germany, 2015.
19. Oikonomou, K.; Roh, H.; Reinhorn, A.M.; Schiff, A.; Kempner, L. Seismic performance evaluation of high voltage transformer bushings. *Struct. Congr.* **2010**, *2010*, 2724–2735.
20. Yang, J.; Rustogi, S.K.; Gupta, A. Rocking stiffness of mounting arrangements in electrical cabinets and control panels. *Nucl. Eng. Des.* **2003**, *219*, 127–141. [CrossRef]
21. Filiatrault, A.; Matt, H. Experimental Seismic Response of High-Voltage Transformer-Bushing Systems. *Earthq. Spectra* **2005**, *21*, 1009–1025. [CrossRef]
22. Cao, M.G.; Cheng, Y.F.; Dai, Z.B.; Zhou, F.L.; Tan, P. Parameter Analysis and Shaking Table Test on Seismic Isolation System of Transformer with Bushings. In Proceedings of the 15th World Conference of Earthquake Engineering (WCEE), Lisbon, Portugal, 24–28 September 2012.
23. Chun, N.H.; Jeon, B.G.; Kim, S.W.; Chang, S.J.; Son, S.W. Seismic response evaluation of 154 kV transformer porcelain bushing by shaking table tests. *Struct. Eng. Mech.* **2022**, *84*, 155–165.
24. Jeon, B.G.; Jung, C.Y.; Jin, J.W.; Kim, H.H.; Cheung, J.H. Seismic performance evaluation of 500 kV EBA. *Trans. Korean Soc. Noise Vib. Eng.* **2015**, *25*, 496–502. [CrossRef]
25. Soto, D.O.; Angulo, E.R. Tiempo de interrupción de negocios en la Ciudad de México por daños directos y efectos indirectos en edificios a causa del sismo del 19S de 2017. *Rev. De Ing. Sismica* **2020**, *104*, 1–31.
26. Fujisaki, E. Seismic Performance of Electric Transmission Systems. In Proceedings of the Pacific Earthquake Engineering Research Center 2009 Peer Annual Meeting, San Francisco, CA, USA, 15–16 October 2009.
27. Fallahi, K. Study of Seismic Damage to Power Generation and Distribution Network and Remedy for Improving the Existing Safety Criteria. In Proceedings of the 13th World Conference on Earthquake Engineering, Vancouver, BC, Canada, 1–6 August 2004.
28. Çetin, K.O.; Bray, J.D.; Frost, J.D.; Hortacsu, A.; Miranda, E.; Moss, R.E.; Stewart, J.P. *February 6, 2023 Türkiye Earthquakes: Report on Geoscience and Engineering Impacts: Report No. GEER Association Report 082*; Earthquake Engineering Research Institute (EERI): Berkeley, CA, USA, 2023.
29. Schiff, A.J. *The Lorna Prieta, California, Earthquake of October 17, 1989-Lifelines*; United States Government Publishing Office: Washington, DC, USA, 1998.
30. Bellerive, J.M. *Haiti Earthquake PDNA: Assessment of Damage, Losses, General and Sectoral Needs*; Annex to the Action Plan for National Recovery and Development of Haiti: Port-au-Prince, Haiti, 2010.
31. Institute of Electrical and Electronics Engineers (IEEE). *Recommended Practice for Seismic Qualification of Class 1E Equipment for Nuclear Power Generating Station: IEEE 344*; IEEE: Piscataway, NJ, USA, 1987.
32. Seismic Research and Test Center (SESTEC). *Seismic Qualification Test Report of 500 kV Termination on Support*; Report No. 2014-R-094; SESTEC: Yangsan, Republic of Korea, 2014.
33. Seismic Research and Test Center (SESTEC). *Seismic Qualification Test of Outdoor Sealing End for 230kV XLPE Power Cable*; Report No. SESTEC-2017-R-016-Rev.0; SESTEC: Yangsan, Republic of Korea, 2017.
34. Bandyopadhyay, K.K.; Hofmayer, C.H.; Kassir, M.K.; Pepper, S.E. *Dynamic Amplification of Electrical Cabinets: NUREG/CR-5203*; Nuclear Regulatory Commission: Washington, DC, USA, 1988.
35. *IEEE 693-2018*; Recommended Practice for Seismic Design of Substations. IEEE: Piscataway, NJ, USA, 2018.
36. Chang, S.J.; Jeong, Y.S.; Eem, S.H.; Choi, I.K.; Park, D.U. Evaluation of MCC seismic response according to the frequency contents through the shake table test. *Nucl. Eng. Technol.* **2021**, *53*, 1345–1356. [CrossRef]